International Journal of Minerals, Metallurgy and Materials
Volume 25, Number 6, June 2018, Page 696
https://doi.org/10.1007/s12613-018-1617-4

Mechanisms of reactive element Y on the purification of K4169 superalloy during vacuum induction melting

Qing-ling Li[1)], *Hua-rui Zhang*[1)], *Ming Gao*[1)], *Jin-peng Li*[1)], *Tong-xiao Tao*[2)], *and Hu Zhang*[1)]

1) School of Materials Science and Engineering, Beihang University, Beijing 100191, China
2) Qingdao Institute of New Material Technology of Beihang University, Qingdao 266000, China
(Received: 15 October 2017; revised: 31 January 2018; accepted: 12 February 2017)

Abstract: The effects of rare earth element Y on the purification of K4169 superalloy during vacuum induction melting were investigated at different superheating temperatures. The corresponding interaction mechanisms were also clarified. Results showed that the addition of Y remarkably promoted the purification effect on the K4169 melt. The contents of O and S in the K4169 as-cast alloy ingots after purification were 3–4 and 8–10 ppm, respectively. The degrees of deoxidation and desulfurization increased to 50% and 57%, respectively, upon the addition of 0.1wt% Y. The yttrium-rich phase that precipitated at the grain boundary blocked the diffusion of C and the accumulation of S, thereby contributing to the purification of the alloy.

Keywords: K4169 superalloy; deoxidation; desulfurization; yttrium; vacuum induction melting; mechanism

1. Introduction

Nickel-based superalloys are a distinct class of metallic materials that exhibit good corrosion resistance, high strength, remarkable machinability, outstanding weldability, and microstructural stability at high temperatures (about 650°C) [1–4]. These materials are extensively employed in aircraft and power generation turbines, rocket engines, and other challenging environments, including nuclear power and chemical processing plants [5–6]. Typical nickel-based superalloys usually consist of 10 to 15 different elements, such as Ni, Cr, Co, W, Ta, Al, Mo, Hf, Ti, Re, and Ru [7]. Such high degree of alloying makes the nickel-based superalloys extremely form element segregation, and the content of gas and impurity elements in the alloy matrix is strictly controlled. Many works have investigated the negative influences of impurities on the microstructure and properties of cast nickel-based superalloys [8–10].

In general, trace amounts of harmful elements, namely, O, N, and S, in the superalloy matrix, even at low concentrations (ppm level), could cause the formation of inclusions and the initiation and propagation channels of fatigue cracks, which adversely affect the creep and endurance strength of superalloys [11]. According to Miller *et al.* and Sadananda *et al.* [12–13], trace O increased the crack growth rate in Inconel 718 at high temperatures by up to 4.5 orders of magnitude over those observed in an inert environment. Sarioglu *et al*. and Simpson *et al.* [14–15] reported that S in superalloys destroyed the high temperature resistant coating and reduced adhesion between the coating and the alloy matrix. For instance, in the case of Inconel 718, when the S content increased from 56 to 175 ppm, the durable life of the alloy was reduced by 68%; when the S content increased from 15 ppm to 50 ppm, the elongation of the alloy decreased from 10% to 5% [16]. Therefore, special methods must be developed for melting nickel-based superalloys and easily restraining the increase in the amount of trace harmful elements in the alloy matrix [17].

Vacuum induction melting (VIM) uses electromagnetic induction heating and controls the melt at the refining process temperature under stirring to obtain ingots with excellent chemical properties and microstructural homogeneity. VIM is one of the most popular methods for melting nickel-based superalloys [18].

Corresponding author: Hua-rui Zhang E-mail: huarui@buaa.edu.cn; Hu Zhang E-mail: zhanghu@buaa.edu.cn

Studies on VIM reported that the addition of a moderate amount of Y contributed to optimization of microstructure and improvement of the anti-oxidation performance and fracture life of nickel-based superalloys [17,19]. Li *et al.* [20] stated that the addition of 0.05wt% Y to GH3535 superalloy increased the hardness of the alloy by about 30%. According to the report of Zhou *et al.* [21], the addition of Y increases the stress rupture life of a Ni-based superalloy, and the stress rupture life peaks when the Y content reaches 0.013wt%. The research of Song *et al.* [22] showed that the oxidation resistance of a Ni-based superalloy was improved by adding proper amount of Y.

The addition of Y during melting of superalloys presents several limitations. As an active rare earth element, Y added to a superalloy may lead to strong reactions of the melt with traditional crucible materials, such as magnesium oxide and calcium oxide, during VIM [23]. The subsequent increase in the contents of harmful elements, such as O, N, and S, would cause the deterioration of the performance of the alloy. Therefore, a suitable crucible material must be selected for remelting of Y-added nickel-based superalloys to restrain the contents of impurity elements.

Previous works showed that Y_2O_3 crucibles with higher chemical stability than traditional MgO crucibles can reduce the interface reaction; as such, Y_2O_3 crucibles have been successfully used and regarded as an ideal crucible for smelting high active alloys containing Y, Ti, Hf, and other active elements [24]. A recent study indicated that the contents of O and N decreased from 24 to 8 ppm and from 28 to 8 ppm, respectively, at 1873 K when a Y_2O_3 crucible was used in the VIM of GH4169 alloy [23]. In addition, Y was considered favorable to the purification of O, N, and S in molten alloys. However, the interaction mechanism among Y, O, and S in nickel-based superalloys remains unclear.

In this study, K4169 superalloy added with 0 to 0.1wt% Y was refined through VIM using Y_2O_3 crucibles. The microstructure of the alloy matrix containing different contents of Y was investigated. The effects of deoxidation and desulfurization of the alloy added with different levels of Y were compared, and the corresponding interaction mechanisms between O and S in the alloy melt and Y were clarified.

2. Experimental

The nominal composition of K4169 superalloy is shown in Table 1. Different contents of rare earth element Y (0, 0.005wt%, and 0.1wt%) were added to the alloy. The alloy ingots were obtained by VIM in a 100-kW ZG125C VIM furnace. Before melting, the chamber was evacuated to the vacuum pressure of 3.5×10^{-3} Pa and backfilled with pure argon (O_2 < 10 ppm; N_2 < 50 ppm; H_2 < 5 ppm; and CH_4 < 4 ppm) up to 0.05 MPa for three times to reduce the O content to a minimum level and avoid the evaporation of alloy components. The superheating temperatures used were 1550, 1600, and 1700°C. The refining time was set as 10 min, and the pouring temperature was 1480°C (measured and controlled by an IR thermometer). The Y_2O_3 ceramic crucibles with a purity of 99% were prepared by cold isostatic pressing at 180 MPa and sintered in a vacuum resistance furnace at 2000°C.

Table 1. Nominal element composition of K4169 superalloy

wt%

C	Cr	Ni	Co	Mo	Al	Ti	Fe	Nb	Ta	B	Zr
0.05	20	55	0.8	3.0	0.7	1.0	Balance	5.0	0.7	0.004	0.04

Samples for characterization and impurity measurement were collected through mechanical separation of the mini ingot from the as-cast alloy ingot. The contents of O and S in the alloy ingot were determined through the infrared thermal conductivity method with inert gas (according to GB/T 11261–2006) and the high-frequency combustion-infrared method (according to GB/T 20123–2006), respectively. The content of Y was measured according to the standard of NACIS/CH 138:2013. The microstructures of the specimens were observed by electron probe microanalysis (EPMA, JOEL, JXL-8100, Japan) and scanning electron microscopy (SEM, JEM-2100, Japan) equipped with energy-dispersive spectroscopy (EDS) and electron backscatter diffraction (EBSD) detectors. Phase analysis was conducted on a microcell X-ray diffractometer (XRD, D/MAX2200pc).

3. Results

3.1. Effects of Y on deoxidation

Table 2 shows the content of O in the K4169 as-cast alloy ingots, which were obtained by adding different amounts of rare earth element Y and subjecting to superheating temperatures of 1550, 1600, and 1700°C. The content of O decreased with increasing Y addition. At the superheating temperature of 1600°C, the decreasing trend of O content was distinct. In this case, the O content of the alloy decreased from 12 to 6 ppm as the amount of Y added was increased from 0 to 0.1wt%. At 1550 and 1700°C, the content of O decreased from 8 to 4 ppm and from 7 to 3 ppm, respectively, as the amount of Y added was increased from 0 to 0.1wt%.

Table 2. O and S contents in alloys added with different amounts of Y at different superheating temperatures ppm

Addition	1550°C		1600°C		1700°C	
of Y / wt%	O	S	O	S	O	S
0	0.0008	0.0016	0.0012	0.0015	0.0007	0.0015
0.005	0.0005	0.0013	0.0011	0.0014	0.0006	0.0014
0.1	0.0004	0.0011	0.0006	0.0008	0.0003	0.0010

Fig. 1 illustrates the influences of Y addition on deoxidation during VIM at different superheating temperatures. At a low temperature (1550°C), the deoxidation rate in the ingot added with 0.005wt% Y increased by 37.5% compared with that in the yttrium-free alloy ingot. The deoxidation rate in the ingot increased by 50% when the amount of Y added was increased from 0 to 0.1wt% and by 8.3% (1600°C) and 14.28% (1700°C) upon adding 0.005wt% Y. When the amount of Y added was increased to 0.1wt%, the deoxidation rate significantly increased to 50% (1600°C) and 57% (1700°C).

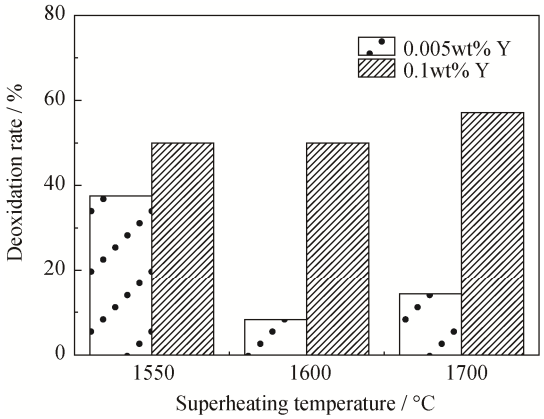

Fig. 1. Deep deoxidation degree of alloys added with different amounts of Y at different temperatures.

3.2. Effects of Y on desulfurization

As shown in Table 2, the contents of S in the alloy without Y were 16 (1550°C), 15 (1600°C), and 15 ppm (1700°C). When the amount of Y added was 0.1wt%, the S content decreased to 11 (1550°C), 10 (1600°C), and 8 ppm (1700°C). Moreover, the S content in each alloy was mostly identical at different superheating temperatures, indicating that the temperature probably had no obvious effect on desulfurization in VIM.

Fig. 2 shows the influence of Y addition on desulfurization in VIM at different superheating temperatures. The effect of Y content on desulfurization rate was consistent with its influence on deoxygenation rate. At a low temperature (1550°C), adding 0.005wt% Y increased the desulfurization rate by 18.75%; further increase in the amount of Y exerted minimal effect on the desulfurization rate. At high temperatures (1600 and 1700°C), adding 0.005wt% Y had no effect on the desulfurization rate. When the amount of Y added was increased to 0.1wt%, the desulfurization rate was remarkably improved.

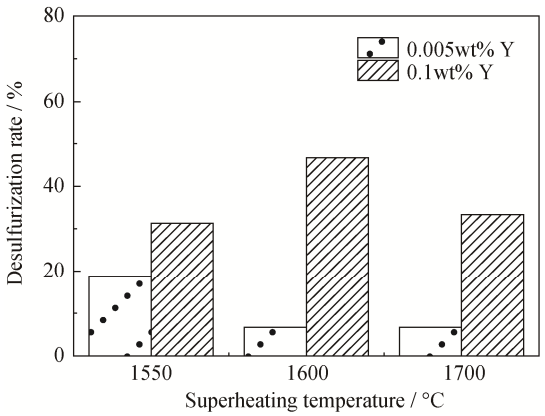

Fig. 2. Deep desulfurization degree of alloys added with different amounts of Y at different temperatures.

3.3. Microstructure

Fig. 3 shows the microstructure of K4169 alloy added with different contents of Y at different superheating temperatures. As shown in the microstructure pictures (Figs. 3(a), 3(d), 3(g), and 4(a)), the alloy without Y possessed an irregular white precipitate, which was found to be the Laves phase. Few acicular delta phases were also found around the Laves phase, and a large number of irregular, blocky, or round granular carbides were detected. Based on further analysis by the microcell XRD peak spectrum (Fig. 5), the carbides were mainly Nb_2C and NbC. When the amount of Y added was 0.005wt%, the SEM images (Figs. 3(b), 3(e), and 3(h)) showed inconspicuous phase change of the precipitates in the alloy; this finding was basically the same as that in alloys without Y. When the amount of Y added was increased to 0.1wt% (Figs. 3(c), 3(f), 3(l), and 4(b)), the morphology of carbides in the precipitated phase of K4169 changed from small particles with a diameter of 2 to 4 μm to long strips with the size of 5 to 20 μm. In addition, the size of the island-like or screen-like Laves phase increased.

Fig. 6(a) shows the TEM image of yttrium-rich phase observed in the alloy added with 0.1wt% Y. When the amount of Y added was 0.1wt%, the yttrium-rich phase was precipitated at the grain boundary. Based on the diffraction spots (Fig. 6(b)) and the atomic ratio, the phase was determined to be Y_2Ni_7. In addition, carbides precipitated near the yttrium-rich phase. However, in samples without Y and added with 0.005wt% Y, only the precipitated phase of carbide was observed at the grain boundary without the Y phase.

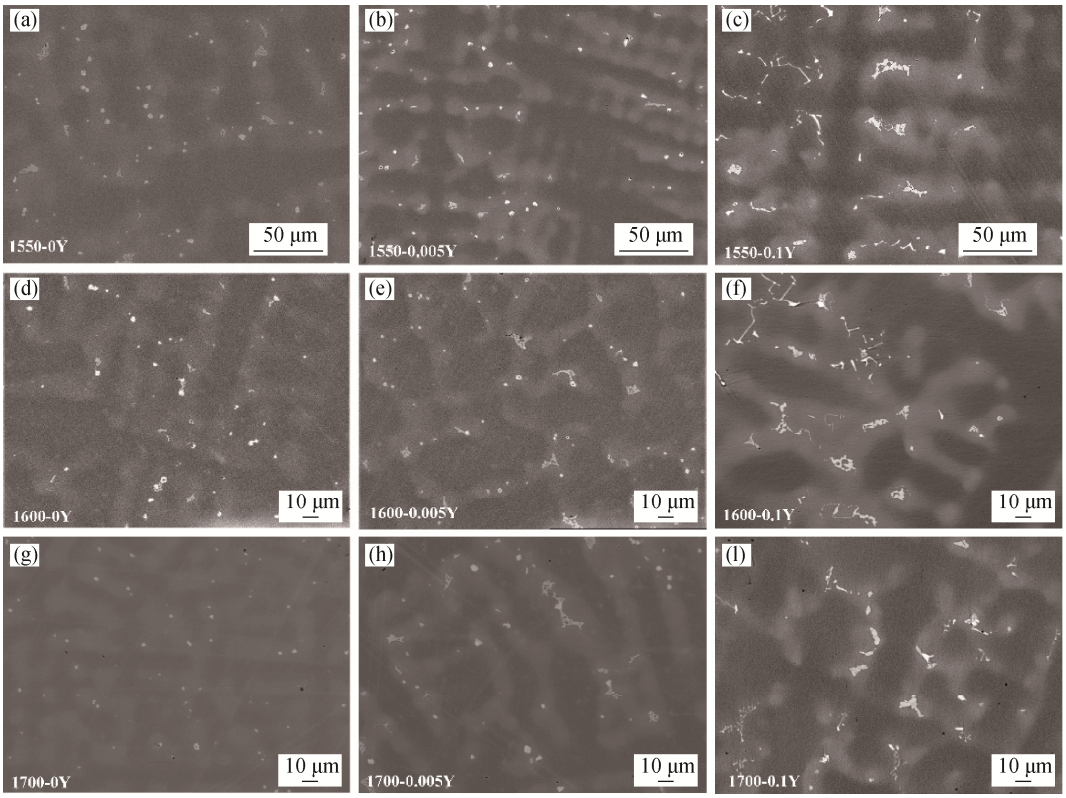

Fig. 3. Microstructure of the samples added with various amounts of Y at different superheating temperatures: (a, b, c) 1550°C; (d, e, f) 1600°C; (g, h, l) 1700°C.

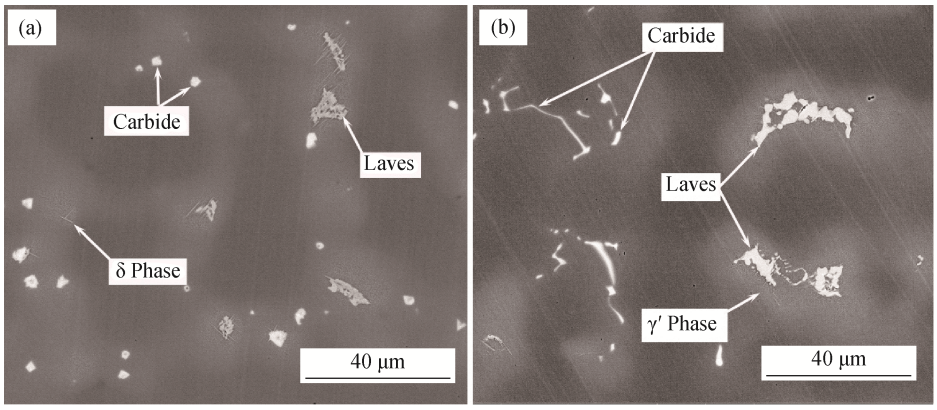

Fig. 4. Microstructure of the samples at a superheating temperature of 1700°C: (a) 0wt% Y; (b) 0.1wt% Y.

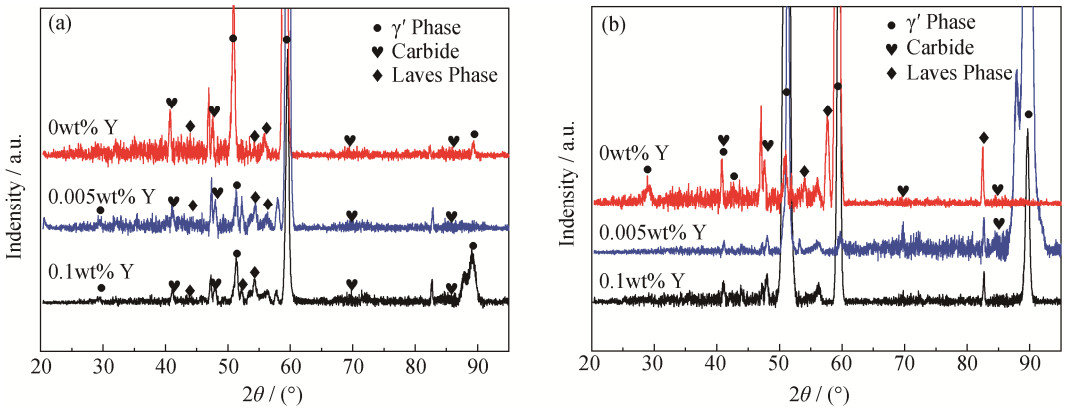

Fig. 5. Microcell XRD diagram of the samples at 1600 (a) and 1700°C (b).

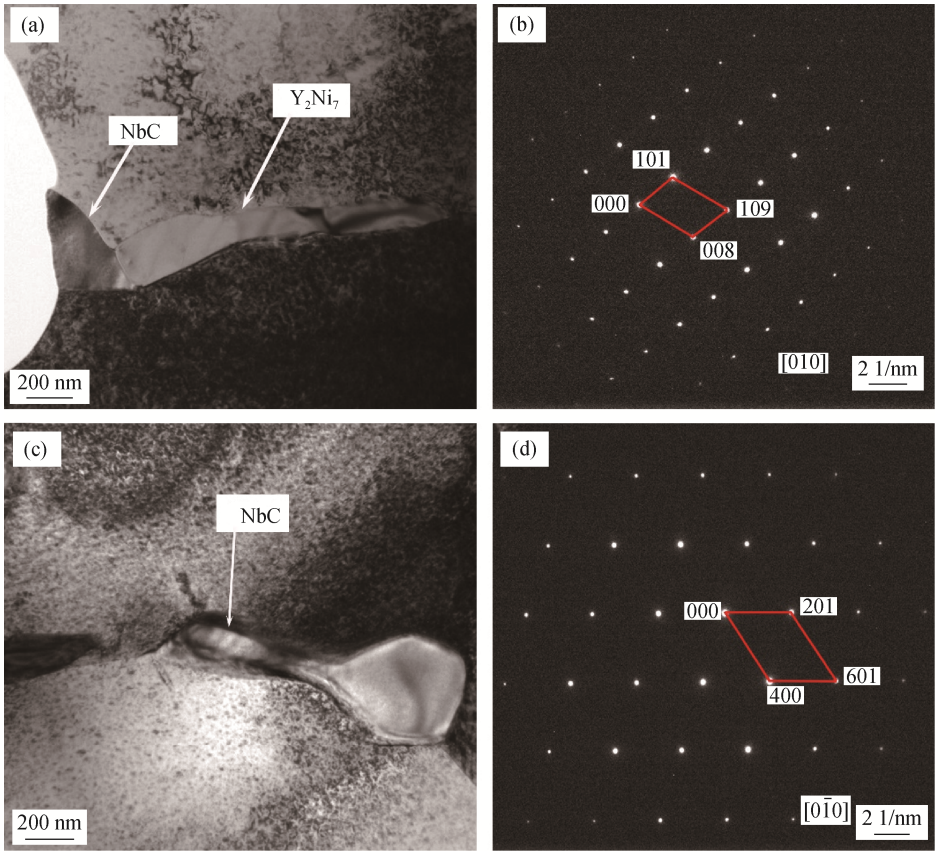

Fig. 6. TEM images of the sample added with 0.1wt% Y at 1700°C (a, c), and diffraction spots of Y_2Ni_7 (b) and NbC (d), respectively.

4. Discussion

The addition of Y remarkably promoted the purification of O in the K4169 alloy melt during VIM. The deoxidation effect on the K4169 as-cast alloy ingots decreased from 12 ppm to 3–4 ppm when Y was added to the alloy. Moreover, the deoxidation rate increased with increasing content of Y and superheating temperatures. Carbon deoxidization was found to be the main deoxidation mechanism considering that 0.05wt% C was added to the alloy in the early stage of melting (Table 1). In the later stage of melting, Al and Y were added to the alloy, and the main deoxidation reactions are shown in Table 3. Compared with standard free energy levels of C/O and Al/O, Y/O presents the most negative standard free energy of the reaction. Upon adding a small amount of Y to the alloy, this element will preferentially react with O to generate Y_2O_3 before C/O and Al/O reactions.

Table 3. Major deoxidation reactions in K4169 alloy melt

No.	Chemical reaction	Standard free energy, $\Delta G^{\ominus}$ / kJ
(1)	$C + O = CO$	$-67742 - 39.75T$
(2)	$2Al + 3O = Al_2O_3$	$-1158310 + 364.58T$
(3)	$2Y + 3O = Y_2O_3$	$-1792600 + 658T$

For Reaction (3) at a certain temperature:

$$\Delta_r G^{\ominus} = -RT\ln K = -2.303RT\lg K \tag{4}$$

Equilibrium constant K can be expressed as:

$$K = \frac{a_{Y_2O_3}}{a_O^3 a_Y^2} = \frac{a_{Y_2O_3}}{[f_O(\%O)]^3[f_Y(\%Y)]^2} \tag{5}$$

where K is the equilibrium constant; $\Delta G^{\ominus}$ is the standard Gibbs free energy; f_Y and f_O are the activity coefficients of Y and O in the melt of nickel-based superalloy; and %O is the solid solubility of O in the liquid melt. The melting point of pure Y_2O_3 is higher than 2400°C [23]; thus, $a_{Y_2O_3} = 1$ is taken. In the multi-alloy system, the activity coefficient can be expressed by the first- and second-order interaction coefficients of Wagner the effect of alloying elements on N solubility in the alloy.

$$\lg f_O = e_O^O[\%O] + e_O^{X_i}[\%O_i] + r_O^{X_i}[X_i]^2 \tag{6}$$

where e_O^O is the interaction coefficient of O, $e_O^{X_i}$ and $r_O^{X_i}$ are the first- and second-order interaction coefficients, respectively; and $[X_i]$ is the solubility of alloy element i.

In most cases, the zero- and first-order interaction coefficients are used to meet accuracy requirements.

$$\lg f_O = e_O^O[\%O] + e_O^{X_i}[\%O_i] \tag{7}$$

According to the calculation, $f_O = 0.898$. The activity coefficient of Y f_Y is equal to 1. Fig. 7 shows the relationship between the amount of Y added and the O content in the alloy at different superheating temperatures (1550, 1600, and 1700°C).

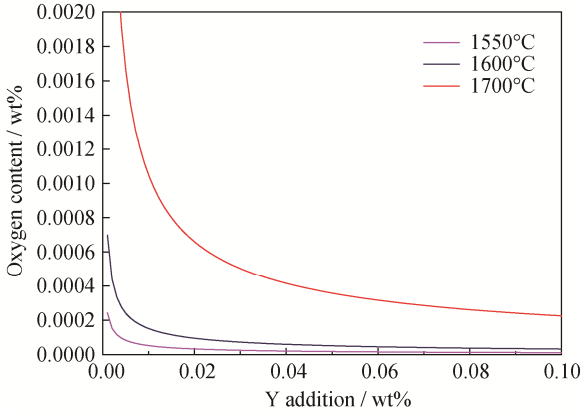

Fig. 7. Theoretical calculation of the relationship between Y addition and O content in the alloy.

With the addition of Y, the O content in the molten alloy decreased sharply and slowly converged to a minimum level at a certain superheating temperature. The calculated results coincide with the experimental results in the study. Comparison of the experimental results and the calculated values indicated that the O content in the K4169 alloy was higher than the theoretical value. This finding could be due to the fact that the calculation result was fully based on the actual amount of Y added and that its evaporation during the remelting process was not considered. Thus, the actual amount of Y was slightly lower than the designated amount. Based on the downward trend of the curve in Fig. 7, when the amount of Y was increased, the decrease in the O content at low temperatures was more obvious than that at high temperatures. Hence, at a low superheating temperature of 1550°C, the great increase in deoxidation rate could be obtained by adding even a small amount of Y (0.005wt%). When the amount of Y added was 0.1wt%, the highest deoxidation rate was obtained at high temperatures (1600 and 1700°C).

In addition to O, the addition of Y significantly affected the purification of S. The desulfurization degree increased when the amount of Y added was increased to 0.1wt%. According to the report of Li *et al.* [25], the desulfurization reaction can be expressed as

$$[S]+(O^{2-})=(S^{2-})+[O] \quad (8)$$

$$\Delta_r G^{\ominus} = -20110+3.44T \quad (9)$$

Alkaline slag is beneficial to desulfurization; the Y added and O in the molten metal form the basic oxide Y_2O_3 [26], which improved the alkalinity of the slag and was favorable for desulfurization. Given the low amount of Y added, the formation of Y_2O_3 was limited, and the decrease in the S content seemed quite significant. According to the report of Sun *et al.* [27], S was preferentially distributed in the metal carbide of MC and grain boundaries of the alloy. The corresponding schematic is shown in Fig. 8. The atomic radius of Y (0.18 nm) is larger than those of Fe, Co, and Ni (0.124–0.128 nm); as such, the distortion energy in the crystal can be greater than that at the grain boundary, resulting in the precipitation of Y. Based on the TEM image of the sample added with 0.1wt% Y (Fig. 6), the yttrium-rich phase precipitated. The segregation of Y blocked the diffusion of carbon and the accumulation of S at the grain boundary, leading to uneven aggregation of carbides in the alloy added with Y and reduction in the S content. Therefore, Y addition could be helpful to desulfurization of alloy melts.

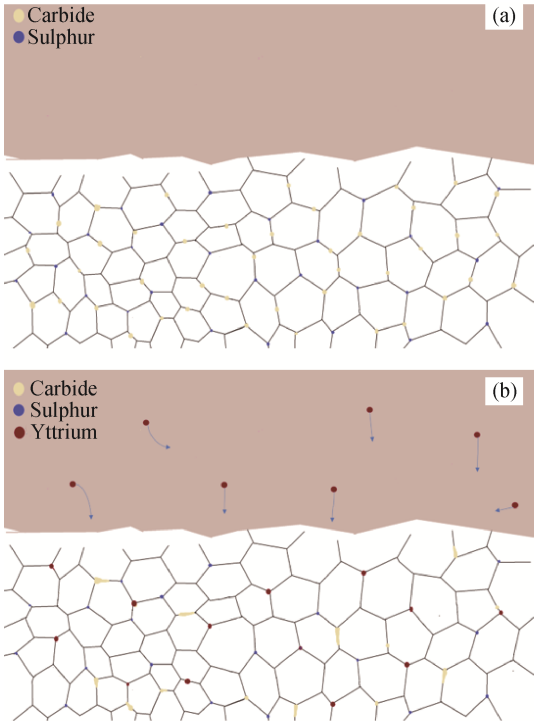

Fig. 8. Schematic of Y occupying the position of grain boundaries.

5. Conclusions

The effects of adding 0, 0.005wt%, and 0.1wt% Y on the deoxidation and desulphurization of K4169 superalloy in VIM at different superheating temperatures were discussed. The corresponding interaction mechanisms were clarified. The primary conclusions of this work are as follows:

(1) The addition of rare earth element Y remarkably promoted the purification effect on the K4169 melt. The contents of O and S in the K4169 as-cast alloy ingots after purification were 3–4 and 8–10 ppm, respectively, upon the addition of 0.1wt% Y.

(2) The degrees of deoxidation and desulfurization were 50% and 57%, respectively, in the alloy added with 0.1wt% Y compared with those in the alloy melt without Y. At a low temperature of 1550°C, adding a low amount of Y (0.005wt%) increased the deoxidation and desulfurization rates by 37.5% and 18.75%, respectively. When the temperature was increased to 1600 and 1700°C, the deoxidation and desulfurization rates further increased.

(3) The addition of a small amount of Y did not affect the microstructure of the alloy. When the amount of Y added was increased to 0.1wt%, dispersed granular carbides accumulated at grain boundaries and grown into strips. Meanwhile, the yttrium-rich phase precipitated at the grain boundaries.

Acknowledgements

This work was financially supported by the National Science & Technology Pillar Program of China (No. 2013BAB11B04) and the National Natural Science Foundation of China (Nos. 51404017 and 51604014). Furthermore, the authors wish to express their appreciation to the State Key Laboratory of Refractories and Metallurgy, Wuhan University of Science and Technology.

References

[1] A. Iturbe, E. Giraud, E. Hormaetxe, A. Garay, G. Germain, K. Ostolaza, and P.J. Arrazola, Mechanical characterization and modelling of Inconel 718 material behavior for machining process assessment, *Mater. Sci. Eng. A*, 682(2017), p. 441.

[2] D.H. Ping, Y.F. Gu, C.Y. Cui, and H. Harada, Grain boundary segregation in a Ni–Fe-based (Alloy 718) superalloy, *Mater. Sci. Eng. A*, 456(2007), No. 1-2, p. 99.

[3] G.A. Zickler, R. Schnitzer, R. Radis, R. Hochfellner, R. Schweins, M. Stockinger, and H. Leitner, Microstructure and mechanical properties of the superalloy ATI Allvac® 718Plus™, *Mater. Sci. Eng. A*, 523 (2009), No. 1-2, p. 295.

[4] D.K. Das, V. Singh, and S.V. Joshi, High temperature oxidation behaviour of directionally solidified nickel base superalloy CM–247LC, *Mater. Sci. Technol.*, 19(2013), No. 6, p. 695.

[5] E.C. Caldwell, F.J. Fela, and G.E. Fuchs, The segregation of elements in high refactory-content single-crystal nickel-based superalloys, *JOM*, 56(2004), No. 9, p. 44.

[6] A.J. Brand, K. Karhausen, and R. Kopp, Microstructural simulation of nickel base alloy Incone* 718 in production of turbine discs, *Mater. Sci. Technol.*, 12(1996), No. 11, p. 963.

[7] T.M. Pollock and S. Tin, Nickel-based superalloys for advanced turbine engines: chemistry, microstructure and properties, *J. Propul. Power*, 22(2006), No. 2, p. 361.

[8] V.V. Sidorov, V.E. Rigin, P.G. Min, and Y.I. Folomeikin, Removal of a sulfur impurity from complex nickel melts in vacuum, *Russ. Metall.*, 2015(2015), No. 11, p. 910.

[9] H. Naffakh-Moosavy, Microstructural evolution and castability prediction in newly designed modern third-generation nickel-based superalloys, *Int. J. Miner. Metall. Mater.*, 23(2016), No. 5, p. 548.

[10] L. Wang, Y. Wang, Y. Liu, X. Song, X.D. Lü, and B.J. Zhang, Coarsening behavior of γ′ and γ″ phases in GH4169 superalloy by electric field treatment, *Int. J. Miner. Metall. Mater.*, 20(2013), No. 9, p. 861.

[11] W.X. Yu and J.P. Niu, Deoxidation and denitrogenation during VIM refining Ni-base superalloy, *New Technol. New Process*, 2002, No. 3, p. 32.

[12] C.F. Miller, G.W. Simmons, and R.P. Wei, Mechanism for oxygen enhanced crack growth in inconel 718, *Scripta Mater.*, 44(2001), No. 10, p. 2405.

[13] K. Sadananda and P. Shahinian, The effect of environment on the creep crack growth behavior several structural alloys, *Mater. Sci. Eng.*, 43(1980), No. 2, p. 159.

[14] C. Sarioglu, C. Stinner, J.R. Blachere, N. Birks, F.S. Pettit, G.H. Meier, and J.L. Smialek, The control of sulfur content in nickel-base, single crystal superalloys and its effects on cyclic oxidation resistance, *Superalloys*, 1996, p. 71.

[15] T.M. Simpson and A.R. Price, Oxidation improvements of low sulfur processed superalloys, *Superalloys*, 2000, p. 387.

[16] J.X. Dong, X.B. Liu, B. Tang, Y.H. Hu, Z.C. Xu, and X.S. Xie, Effects of S on mechanical properties and microstructure of Inconel 718 alloy, *Acta Metall. Sin.*, 32(1996), No. 3, p. 241.

[17] L.V. Ramanathan, Role of rare-earth elements on high temperature oxidation behavior of FeCr, NiCr and NiCrAl alloys, *Corros. Sci.*, 35(1993), No. 5-8, p. 871.

[18] N. Nayan, Govind, C.N. Saikrishna, K.V. Ramaiah, S.K. Bhaumik, K.S. Nair, and M.C. Mittal, Vacuum induction melting of NiTi shape memory alloys in graphite crucible, *Mater. Sci. Eng. A*, 465(2007), No. 1-2, p. 44.

[19] X.H. Cheng, L. Fan, L. Li, K.F. Du, and D.H. Wang, Effect of doping aluminum and yttrium on high-temperature oxidation behavior of Ni–11Fe–10Cu alloy, *J. Rare Earths*, 34(2016), No. 11, p. 1139.

[20] X.L. Li, S.M. He, X.T. Zhou, Y. Zou, Z.J. Li, A.G. Li, and X.H. Yu, Effects of rare earth yttrium on microstructure and properties of Ni–16Mo–7Cr–4Fe nickel-based superalloy, *Mater. Charact.*, 95(2014), p. 171.

[21] P.J. Zhou, J.J. Yu, X.F. Sun, H.R. Guan, X.M. He, and Z.Q. Hu, Influence of Y on stress rupture property of a Ni-based superalloy, *Mater. Sci. Eng. A*, 551(2012), p. 236.

[22] L.G. Song, S.S. Li, Y.R. Zheng, and Y.F. Han, Effect of yt-

trium on high temperature oxidation resistance of a directionally solidified superalloy, *J. Rare Earths*, 22(2004), No. 6, p. 794.

[23] H.B. Bai, H.R. Zhang, J.F. Weng, B. Kong, and H. Zhang, Purification behaviour of GH4169 scraps under argon atmosphere during vacuum induction melting, *Mater. Res. Innovations*, 18(2014), No. S4, p. 357.

[24] H.R. Zhang, X.X. Tang, C.G. Zhou, H. Zhang, and S.W. Zhang, Comparison of directional solidification of γ-TiAl alloys in conventional Al_2O_3 and novel Y_2O_3-coated Al_2O_3 crucibles, *J. Eur. Ceram. Soc.*, 33(2013), No. 5, p. 925.

[25] S.J. Li, Y.H. Hu, H.S. Mei, X.S. Xie, Y.H. He, and H.B. Zhang, Desulphurization of Ni-base superalloy GH690, *J. Iron Steel Res.*, 15(2003), No. 7, p. 317.

[26] L.H. Zhao, X.M. Zheng, and J.H. Fei, Surface properties of rare earth oxide solid-base catalysts. Ⅰ. Characterization of surface active sites of rare earth oxide calalysts, *Chin. J. Catal.*, 17(1996), No. 3, p. 227.

[27] C. Sun, R.F. Huang, J.T. Guo, and Z.Q. Hu, Sulphur distribution in K24 cast nickel-base superalloy and its influence on mechanical properties, *High Temp. Technol.*, 6(1988), No. 3, p. 145.